XMM-Newton and *Chandra* High Resolution X-Ray Spectroscopy of Magnetic Cataclysmic Variables and Low Mass X-Ray Binaries

V. Burwitz[1], K. Dennerl[1], F. Haberl[1], P. Predehl[1], K. Reinsch[2], B. Stelzer[3]

[1] MPI für extraterrestrische Physik, Giessenbachstr., D-85748 Garching, Germany, E-mail: *burwitz@mpe.mpg.de*

[2] Universitäts Sternwarte Göttingen, Geismarlandstr. 11, D-37083 Göttingen, Germany

[3] Osservatorio Astronomico di Palermo, Piazza del Parlamento 1, I-90190 Palermo, Italy

ABSTRACT. Here we discuss the helium-like triplet plasma diagnostic method that can be applied to high resolution X-ray spectra of magnetic CVs and low mass X-ray binaries obtained with the high-resolution spectrographs on the ESA satellite *XMM-Newton* and the NASA satellite *Chandra* . The two observations of Her X-1 obtained with the *Chandra* Low Energy Transmission Grating (LETGS), one lasting 30 ks during the anomalous low state (ALS) and the other 20 ks during main on just before eclipse ingress. During the ALS and the pre-eclipse dips only the intercombination line of the He-like O VII and N VI triplets are detected. Thus the resonance line must be scattered out of the line of sight indicating an optical depth of $\tau > 1$. The missing forbidden lines give for collisional plasma a lower limit for density of $n_e > 10^{11...12}\,\mathrm{cm}^{-3}$ and for the temperature of $T \sim 10^{6.0...6.5}\,\mathrm{K}$. These contraints require the corona to be at a distance $r \sim 10^{10-11}\,\mathrm{cm}$ from the central source. *XMM-Newton* RGS spectra during similar states show exactly the same He-like triplet structure as the Chandra observations. For the magnetic CVs AM Her and PQ Gem the most remarcable result is that the lines emitted in the post-shock flow from the cooling hot plasma are strongly broadned. The most likely reason for this is the Doppler-shifting of the lines due to the changing angle between the observer and the accretion column as the white dwarf rotates. The maximum detectable shift in the case of AM her is of the order of 750 km/s.

Key words: Stars: binary: cataclysmic; Stars: binary: LMXBs; stars: individual: AM Her, PQ Gem, Her X-1.

1. Introduction

Modern X-ray observatories such as the European Space Agency (ESA) satellite *XMM-Newton* (Jansen et al. 2001) and the National Aeronautics and Space Agency (NASA) satellite *Chandra* (Weisskopf et al. 2002), which were both launched in 1999, each carry high-resolution X-ray spectrographs onboard. On *XMM-Newton* the Reflection Grating Spectrometers (RGS1, RGS2) and on *Chandra* the Low- and High-Energy Transmission Grating Spectrographs (LETGS and HETGS). Since these instruments have been commissioned they have yielded extraordinary insights into the plasma physics of the many bright galactic and extragalatic sources which have been observed during the past 4 years.

Table 1: Comparison of *XMM-Newton* and *Chandra* .

	XMM-Newton	Chandra
Orbit		
Launch date	Dec. 10, 1999	July 23, 1999
Period (hours)	48	64
Apogee (km)	114000	140000
Mirror Systems		
Type	Wolter 1	Wolter 1
# Modules	3	1
# Mirror/Module	58	4
Focallength (m)	7.5	10.0
Diameters (cm)	30-70	65, 87, 99, 123
Mirror Coating	Gold	Iridium
PSF (FWHM)	$\sim 4.5''$	$\sim 0.5''$
Detectors		
CCDs	EPIC-pn(BI[a])	ACIS-S(2 BI[a],
	EPIC-MOS(FI[b])	4 FI[b])
	RGC1,2(FI[b])	ACIS-I (4 FI[b])
Microchannel-	-	HRC-S (3 det.)
plates	-	HRC-I (1 det.)
Use of detectors	simultaneous	individually
High Resolution Spectrographs		
Spectrograph	RGS1	LETGS
	RGS2	HETGS

[a] BI: Back illuminated CCDs.

[b] FI: Front illuminated CCDs.

With these intruments, especially the high resolution X-ray spectrographs it is possible, to perform detailed studies of the hot X-ray emitting plasmas. This includes the precise determination of the plasma parameters such as temperature, density and also abun-

Table 2: Properties of the the high resolution X-ray spectrographs on *XMM-Newton* and *Chandra* .

	RGS	LETGS	HETG-MEG	HETG-HEG
Wavelength range	5 - 38 Å	1.2-175 Å(HRC-S)	2.5-31 Å	1.2-15 Å
		1.2-65 Å(ACIS-S)		
Energy range	2.5-0.33 keV	10-0.07 keV (HRC-S)	5-0.4 keV	10-0.8 keV
		10-0.2 keV (ACIS-S)		
Resolving power $\lambda/\delta\lambda$	150-800	$20\times\lambda$ (3-50 Å)	970-80	1070-65
		$\geq$1000 (50-160 Å)		
Resolution ($\delta\lambda$,FWHM)	0.06 Å	0.05 Å	0.23 Å	0.12 Å
Effective area (1st order)	RGS1+RGS2	HRC-S , ACIS-S	(MEG+HEG, ACIS-S)	
@ 0.5 keV (24.8Å)	100 cm^2	15 cm^2 , 7 cm^2	3 cm^2	
@ 1.0 keV (12.4Å)	65 cm^2	26 cm^2 , 52 cm^2	48 cm^2	
@ 1.5 keV (8.2Å)	60 cm^2	36 cm^2 , 93 cm^2	150 cm^2	
@ 6.5 keV (1.9Å)	1 cm^2	5 cm^2 , 23 cm^2	25 cm^2	

dances. In section 2 *XMM-Newton* and *Chandra* are compared. Section 3 discusses and compares the high resolution X-ray spectrographs. A description of what can be learnt from the high resolution X-ray spectra is discussed in Section 4. In section 5 and 6 the application of this to the LMXB Her X-1 and the magnetic cataclysmic variables AM Her and PQ Gem is shown.

2. *XMM-Newton* and *Chandra*

In Table 1 the main features of *XMM-Newton* and *Chandra* X-ray observatories are listed. The main strength of *XMM-Newton* Newton is the large collecting are and the highly sensitive back illuminated *EPIC-pn* CCD which together with the other detectors on board allows high-signal to noise CCD spectra to be obtained with relatively short integration times. *Chandra* on the other hand has only one high resolution mirror assembly (HRMA) optimised for obtaining high resolution images with a PSF(FWHM) of 0.5". These detailed images that also contain energy information have yielded fascinating new insights and details on the structure of extended objects in X-rays. The smaller collecting area requires longer integration times.

The high-resolution spectrographs on both satelites are discussed in more detail below.

3. The High Resolution X-ray Spectrographs

3.1. The two RGS on board XMM-Newton

The X-ray satellite *XMM-Newton* has 3 mirror modules which focus the light onto 3 separate imaging arrays, a very sensitive *EPIC-pn* , and two *EPIC-MOS* CCD detectors. Part of the light going to the *EPIC-MOS* detectors encounters the reflection grating elements in the light path and is dispersed to each array of 9 CCDs which detect the high resolution spectra (for details see Table 2). It is also described in detail in van den Herder et al. (2001) On *XMM-Newton* all detectors are usually used simultaneously which allows simultaneous high resolution spectroscopy and high signal-to-noise low resolution broadband spectra to be obtained.

3.2. The LETGS and HETGS on board Chandra

Chandra has one high resolution mirror assembly (HRMA) optimised for high resolution imaging. It can also be used for performing high resolution spectroscopy by mechanically introducing a structure into the convergent light path that holds many small transmission grating facets through which the light exiting the HRMA has to pass. The facets are placed on a so called "toroidal Roland geometry" Beuermann et al. (1979) so that the spectra are formed in the focal plane on the microchannel plate detectors or the CCD arrays. *Chandra* has two sets of grating facets, the LETG which is optimised for the low energy X-rays down to 0.08 keV and the HETG for high energy X-rays up to $\sim$ 8 keV. The HETG is composed of the HEG and MEG grating facets that generate wo sets, of high and medium resolution spectra simultaneously (See Table 2 for details). The LETGS is described in detail in (Brinkman et al. 2000).

4. Plasma Diagnostics from High Resolution spectra

A detailed analysis of the emission lines in the the high resolution X-ray allows to put contraints on the physical parameters such as temperature and density of hot plasma as well as determine its chemical composition. The methods that can be applied will be briefly

Table 3: Summary of *Chandra* Observations of Her X-1

	Obs. ID	Obs. Int.	Exp. [ksec]	Start Date yyyy/mm/dd	Start Time [UT]	Stop Time [UT]	$\Phi_{\rm orb}$	Her X-1 state
(A)	108	0	30.3	2000/02/03	00:49:23	09:38:00	$0.62 - 0.83$	Anom. Low
(B)	108	1	21.6	2001/01/25	03:57:26	10:21:19	$0.68 - 0.83$	Main-On

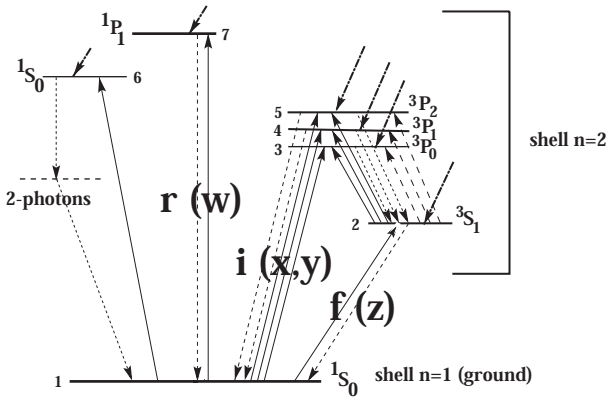

Figure 1: Above is a simplified level scheme for helium-like ions. The characteristic He-like triplet transitions are indicated, with r (or w) the resonance line, i (or x, y) the intercombination line, and f (or x) the forbidden line. (graph taken from Porquet et al. 2001).

described below.

4.1. The Helium-Like Triplets

In the wavelength range (2-175 Å) where the high-resolution spectrographs described above are sensitive one can detect the He-like triplets from different elements (C V, N VI, O VII, Ne IX, Mg XI, and Si XIII). These triplets, the most intense lines of the He-like ions, are composed of the resonance line r (or w), the intercombination line i (or x, y actually at nearly identical wavelength), and the forbidden line f (or x) (ee level scheme in Fig. 3.). They provide a measure for the electron densities and temperatures in the ranges $n \sim 10^{8...13}\,\mathrm{cm}^2$ and $T \sim 1 - 10\,\mathrm{MK}$ respectively as first shown by Gabriel and Jordan (1969). They introduced two ratios for the helium-like triplet lines that are sensitive in specific ranges on the electron density

$$R(n_e) = \frac{f}{i} \qquad (1)$$

and the electron temperature

$$G(T_e) = \frac{f+i}{r} \qquad (2)$$

The range in which these ratios are sensitive to the the density and temperature respectively depends on the the He-like ion triplett lines that are being studied. Generally speaking the lighter the element the lower densities and temperatures at which the G and R ratios are sensitive. This can be clearly seen in detailed graphs given in Porquet and Dubau (2000), Porquet et al. (2001) and Mauche (2002). There are several factors that can complicate the interpretation of the values obtained using these ratios. In addition to collisional excitation a strong UV radiation field can depopulate the level from which the forbidden lines originate so that the strength of the radiation field has to be considered in the calculations. Again these effects are dicussed amply in the papers mentioned above.

5. The low mass X-ray binary Her X-1

Here we present the results from two *Chandra* observations of Her X-1, a $\sim 30\,$ksec exposure during the anomalous low-state and a $\sim 20\,$ksec observation 10 months later in the Main-On (see Table 3). The second LETGS observations of Her X-1 was obtained in Jan 2001 after the source had recovered its 35 d-cycle. The data were acquired during the Main-On before eclipse ingress. This data set shows a series of pre-eclipse dips (see lightcurve below). Pre-eclipse dips result from shadowing of the central X-ray source by the accretion stream.

Her X-1 is a low-mass X-ray binary in a 1.7 d orbit. The spin period of the neutron star is 1.23 s. In addition to these basic periods the X-ray emission from Her X-1 is modulated at a 35 d cycle with two high-states (Main-on and Short-On) separated by $\sim 4\,$d long off-states. From March 1999 to July 2000 Her X-1 was in an anomalous low-state during which the 35 d period disappeared.

These observations allow us for the first time to detect emission, in the form of the intercombination lines of density sensitive He-like O VII and N VI triplets as well as the H-like Lyα O VIII and N VII lines, from the corona above the accretion disc in Her X-1. Both data sets cover nearly the same range in orbital phase which allows for good comparison of the different states.

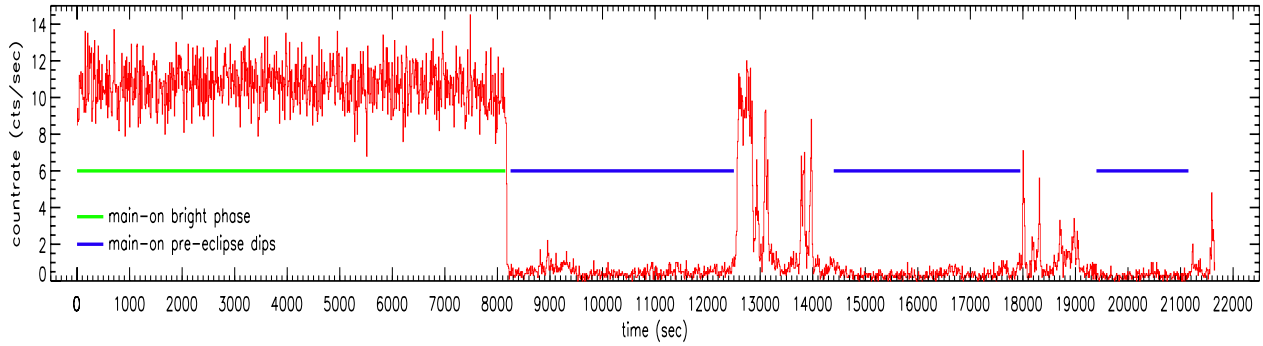

Figure 2: Zeroth order Main-on Lightcurve of Her X-1 with pre-eclipse dips.

5.1 The Her X-1 Data

5.1.1 (A) The anomalous low-state

The LETGS observation of Her X-1 from Feb 2000 was performed while the object was in an anomalous low state (ALS) which at the time had been ongoing since April 1999 (Levine & Corbet 1999, Parmar et al. 1999, Coburn et al. 2000). Previous ALSs in June 1983 and August 1993 where reported by Parmar et al. (1985) and Vrtilek et al. (1994) respectively. During an ALS the region near the accreting neutron star which is responsible for the bright phases in the 35 d-cycle is not visible. This is probably due to changes in the shape (warping, thickness) of the accretion disk.

Thus during such a low state we ought to see mainly X-ray light coming from the corona above/below the inner region of the accretion disk and/or X-rays reprocessed in the irradiated atmosphere of the companion (Basko & Sunyaev 1973). The *Chandra* observation was timed to be performed during phase of maximum brightness of the 35 d-cycle before the eclipse ingress.

5.1.2 (B) The Main-On

A second LETGS observations of Her X-1 was obtained in Jan 2001 after the source had recovered its 35 d-cycle. The data were acquired during the Main-On before eclipse ingress. This data set shows a series of pre-eclipse dips (see lightcurve shown in Fig. 2). Pre-eclipse dips result from shadowing of the central X-ray source by the accretion stream.

5.1.3 The XMM data of Her X-1

From all the *XMM-Newton* observations of Her X-1 that have been performed so far the O VII in (Fig. 3 top right) and the N VI (Fig. 3 bottom right) intercombination lines were best visible in the RGS observations from orbits 509, 510, 516, 603 and orbits 226, 232, 410, 509 respectively.

5.2 The accretion disk corona of Her X-1.

In the Fig. 3 left and center we display the most prominent spectral lines in the LETGS spectrum of Her X-1. During the ALS only the intercombination lines of the O VII and N VI triplet stand out clearly. The forbidden and resonance lines of the O VII triplet are also undetected during the Main-On (both bright phase and pre-eclipse dips). For N VI we detect both the resonance and the intercombination line during the pre-eclipse dips, but only the intercombination line during the bright phase. The H-like Lyα lines of O VII and N VI (not shown in the figure) are marginally detected.

The comparison of the He-like triplets at different states of Her X-1 allows to place constraints on its accretion disk corona: The lack of flux in the resonance line during the anomalous low-state means that this line must be scattered out of the line of sight indicating an optical depth $\tau > 1$. The missing forbidden lines in both O VII and N VI give us lower limits for the density of the plasma of the order of $n_e > 10^{11...12}\,\mathrm{cm}^{-3}$ assuming that collisional processes dominate. However, the strength of the forbidden line can also be reduced by photo-ionization in strong UV fields. The presence of both O VII and N VI also helps to estimate the temperature of the emitting plasma to the range of $T \sim 10^{6.0...6.5}\,\mathrm{K}$. From the constraints on the temperature T and the electron density n_e we find that the corona must be at a distance $r \sim 10^{10-11}\,\mathrm{cm}$ from the central source (see Schandl & Meyer 1994 for the n_e versus r diagram).

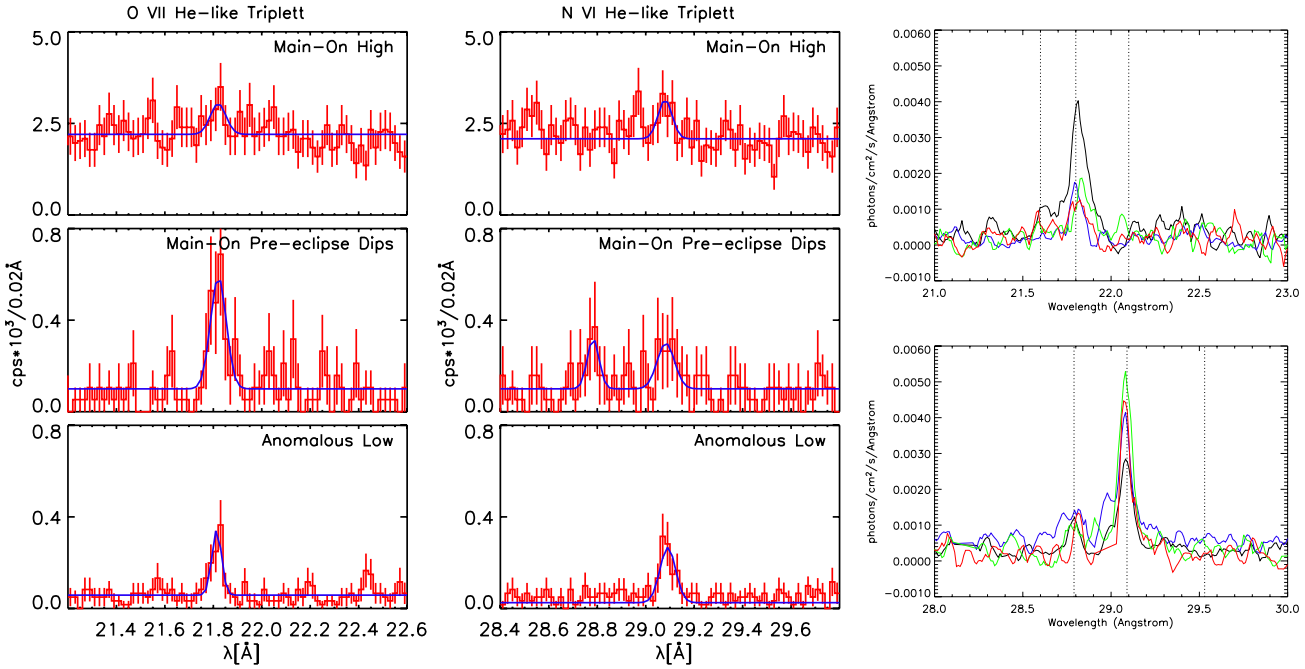

Figure 3: *Left* and *center*: the He-like Tripletts of O VII and N VI during different states of Her X-1 observed using the Chandra LETGS. *right top and bottom* the O VII and N VI He-triplets respectively as observed at different times with the *XMM-Newton* RGS. In all spectra it is clearly visible the the intercombination line is the strongest.

6. The magnetic CVs AM Her and PQ Gem

Here results from our analysis of spin-phase resolved X-ray spectroscopy of the two prototype magnetic CVs, AM Her and PQ Gem are presented. In addition to absorption structures seen in the soft X-ray component of the heated white-dwarf atmosphere individual emission lines of H- and He-like O and N ions including the density sensitive components of the He-like triplets are resolved in the hard X-ray component originating from the post-shock settling flow. Also, phase dependant Doppler-shifts of the emission lines are detected providing detailed information on the geometry of the accretion funnel.

6.1 Chandra LETGS Observations

We have obtained high resolution spin-phase resolved X-ray spectroscopy of the mCVs PQ Gem and AM Her with the *Chandra* LETGS covering the wavelength range 2–170 Å with a spectral resolution $\Delta\lambda$(FWHM) $\sim$ 0.05 Å. PQ Gem and AM Her were observed on Apr. 9, 2000 for 48.8 ksec and on Sep. 30, 2000 for 24.0 ksec, respectively. The data were extracted as described in the *Chandra* proposers guide and in Burwitz et al. (2001a,b,c). Both objects are X-ray bright prototype systems which allow us to study the density, temperature, and geometrical structure of the accretion region in the two physically different environments of a geometrically strongly confined accretion column in the polar AM Her (strong magnetic field-strength case) and a more extended accretion curtain in the intermediate polar PQ Gem (intermediate field-strength case). Here, we present first results of our data analysis.

6.2 Results and discussion

In Burwitz et al. (2001c) a preliminary analysis of the average spectra of PQ Gem and AM Her shows that the temperature sensitive H-like O VIII and N VII emission lines and the density sensitive He-like triplett lines O VII and N VI detected in the spectra are considerably broadened. Phase resolved spectra of AM Her (Fig. 4 left) show that the line broadening is caused by a phase dependant Doppler shift of the emission lines. The maximum detected shift is $\simeq$0.05 Å which at 21.6 Å corresponds to a velocity of $\sim$750 km/s which is compatible with the speeds of the infalling matter in the post-shock flow folded with the changing viewing angle between the accretion pole and the observer. In the case of PQ Gem, the emission line components in the phase-averaged spectra appear to be significantly

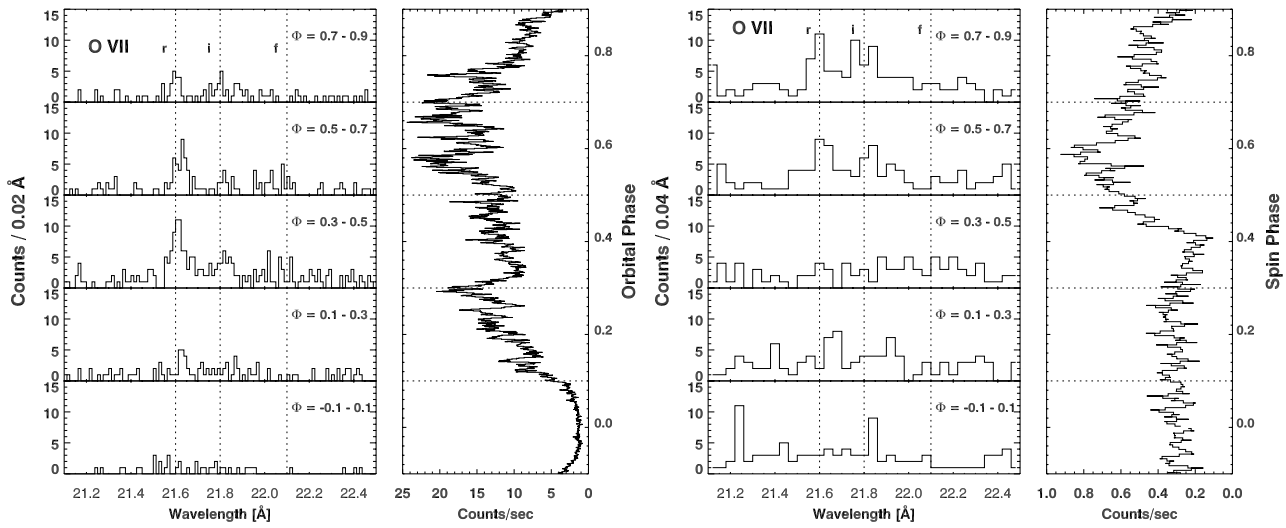

Figure 4: Spin-phase averaged countrate spectra around the density and temperature sensitive OVII Helium-like triplet and the 2–140 Å Phase-folded lightcurve from **left:** the 24.0 ksec Chandra LETGS observation of AM Her and **right:** the 48.8 ksec Chandra LETGS observation of PQ Gem. The nominal positions of the resonance, intercombination, and forbidden lines are labeled.

broader than in AM Her (Fig. 4 right). Such behaviour is expected as in intermediate polars accretion occurs over a much larger range of azimuthal angles than in polars. Hence, at any spin-phase we observe a broader range of projected velocities. Both in AM Her, and PQ Gem the emission lines disappear during the X-ray faint phase.

7. Work on other CVs and LMXBs

In addition to our studies many cataclysmic variables, both magnetic and non magnetic have been studied with *Chandra* especially with the HETGS where Mukai et al.(2003) shows that CVs have two kinds of X-ray spectra. Mauche (2002) discusses high resolution *XMM-Newton* and *Chandra* spectroscopy of the intermediate polar EX Hydrae. Jimenez-Garate et al. 2003 have also worked on Her X-1 data obtained with RGS on *XMM-Newton* .

Acknowledgements. This work has in part been supported by the Deutsches Zentrum für Luft- und Raumfahrt (DLR) grant 50 OX 0001.

References

Beuermann, K., Bräuninger, H., Trümper: 1979 *Appl. Opt.*, **18**, 368.
Basko M. M. & Sunyaev R. A.: 1973, *Ap&SS*, **23**, 117.
Brinkman A.C., Gunsing C.J.T., Kaastra J.S., et al.: 2000 *ApJ* , **530**, 111.
Burwitz V., Zavlin V.E., Neuhäuser R., Predehl P., Trümper J., et al.: 2001a, *A&A*, 379, L35.
Burwitz V., Dennerl K., Haberl F., Neuhäuser R., Predehl P., et al.: 2001b, *ASP Conf Ser.*, **234**, 287.
Burwitz V., Haberl F., Predehl P., Reinsch K., Barwig H.: 2001c, *ASP Conf Ser.*, **251**, 344.
Coburn W., Heindl W. A., Wilms J., et al.: 2000, *ApJ*, **543**, 351.
den Herder, J. W. et al.: 2001, *A&A*, **365**, L7.
Jansen, F., Lumb., D., Altieri, B. et al.: 2001, *A&A*, **365**, L1.
Jimenez-Garate, M. A., Hailey, C. J., Herder, et al.: 2002, *ApJ*, **578**, 391.
Levine A. M., & Corbet R.: 1999, *IAU Circ.*, **7139**.
Mauche, C. W.: 2000, *BAAS 197*, **32**, 1561.
Mauche, C. W.: 2002, *ASP Conf. Ser.*, **261**, 113.
Mukai, K., Kinkhabwala, A., Peterson, J. R., Kahn, S. M., Paerels, F.: 2003, *ApJ*, **586**,77.
Parmar A. N., Oosterbroek T., dal Fiume D., et al.: 1999, *A&A*, **350**, L5
Parmar A. N., Pietsch W., McKechnie S., et al.: 1985, *Nature*, **313**, 119.
Porquet, D. and Dubau J : 2000, *A&AS*, **143**, 495
Porquet, D., Mewe, R., Dubau, J.,Raassen, A. J. J., Kaastra, J. S. : 2001, *A&A*, **376**, 1113.
Schandl S. & Meyer F.: 1994, *A&A*, **289**, 149.
Vrtilek S. D., Mihara T., Primini F. A., et al.: 1994, *ApJ*, **436**, L9.
Weisskopf, M. C., Brinkman, B., Canizares, C., Murray, S., Van Speybroeck, L. P.: 2002, *PASP*, **114**, 1.